Information Content of a Synergy of Ground-Based and Space-Based Infrared Sounders. Part I: Clear-Sky Environments

DAVID M. LOVELESS,[a,b] TIMOTHY J. WAGNER,[b] ROBERT O. KNUTESON,[b] DAVID D. TURNER,[c]
AND STEVEN A. ACKERMAN[a,b]

[a] Department of Atmospheric and Oceanic Sciences, University of Wisconsin–Madison, Madison, Wisconsin
[b] Cooperative Institute for Meteorological Satellite Studies, Space Science and Engineering Center, University of Wisconsin–Madison, Madison, Wisconsin
[c] National Oceanic and Atmospheric Administration/Global Systems Laboratory, Boulder, Colorado

ABSTRACT: Profiles of atmospheric temperature and water vapor from remotely sensed platforms provide critical observations within the temporal and spatial gaps of the radiosonde network. The 2017 National Academies of Science Decadal Survey highlighted that observations of the planetary boundary layer (PBL) from the current space-based observing system are not of the necessary accuracy or resolution for monitoring and predicting high-impact weather phenomena. One possible solution to improving observations of the PBL is supplementing the existing space-based observing system with a network of ground-based profilers. A synthetic information content study is developed utilizing profiles from the Atmospheric Radiation Measurement (ARM) program sites at the Southern Great Plains (SGP), east North Atlantic (ENA), and North Slope of Alaska (NSA) to assess the benefits, in terms of degrees of freedom (DOF), vertical resolution, and uncertainties, of a synergy between the ground-based Atmospheric Emitted Radiance Interferometer (AERI) with space-based hyperspectral infrared (IR) sounders. A combination of AERI with any of the three polar-orbiting IR sounders: the Atmospheric Infrared Sounder (AIRS), the Cross-track Infrared Sounder (CrIS), or the Infrared Atmospheric Sounding Interferometer (IASI), results in a DOF increase of 30%–40% in the surface-to-700-hPa layer compared to the space-based instrument alone. Introducing AERI measurements to the observing system also results in significant improvements to vertical resolution and uncertainties in the bottom 1000 m of the atmosphere compared to CrIS measurements alone. A synergy of CrIS and AERI exceeds the 1-km-vertical-resolution goal set by the Decadal Survey in the lowest 1000 m.

KEYWORDS: Instrumentation/sensors; Profilers, atmospheric; Remote sensing; Satellite observations; Soundings

1. Introduction

Vertical profiles, also known as atmospheric soundings, of temperature and water vapor are critical for the accuracy of numerical weather prediction (NWP; expansions of acronyms may be found in the appendix) (e.g., Langland and Baker 2004; LaRoche and Sarrazin 2010). Radiosonde observations are largely considered the gold standard for atmospheric sounding but are typically taken every 12 h at locations hundreds to thousands of kilometers apart. In situ observations from commercial aircraft and remotely sensed observations are necessary for filling in the temporal and spatial gaps in radiosonde observations. Historically, this is accomplished through the assimilation of radiances from infrared (IR) and microwave (MW) sounders, and GPS radio occultation measurements.

Thermodynamic retrievals derived from the space-based radiance observations measured by MW and IR sounders, such as the NOAA Unique Combined Atmospheric Processing System (NUCAPS; Gambacorta 2013), provide sounding estimates in near–real time to assess atmospheric stability and aid nowcasting of severe convection. However, there are significant errors in satellite-based profiling of the planetary boundary layer (PBL) that limit its applications. Sun et al. (2017) compared the NUCAPS temperature retrieval with radiosonde measurements globally and found differences of

1.5 K at 650 hPa increasing to 3 K at the surface. Another assessment by Nalli et al. (2018) had similar results. These shortcomings in accuracy near the surface result in calculations of convective available potential energy (CAPE) derived from satellite-based retrievals that compare poorly to CAPE calculations from radiosonde profiles (Gartzke et al. 2017; Bloch et al. 2019), thus reducing the utility of satellite profiles. Both studies show that replacing the temperature and water vapor retrieval at the surface with an in situ surface observation provides a significant improvement in correlation of CAPE between radiosonde and retrieval.

Both the National Research Council (NRC) and the National Academy of Sciences (NAS) have highlighted the need for reliable sounding of the PBL in order to improve monitoring and prediction of high-impact weather phenomena. The 2017 Decadal Survey (National Academies of Sciences, Engineering, and Medicine 2018, hereafter referred to as the Decadal Survey) designated that improving observations of the PBL be a priority for future observing missions. The NRC proposed the development of a nationwide network of ground-based profilers to supplement the existing space-based sounding capabilities, in order to improve observations of the PBL (National Research Council 2009). While a network of ground-based profilers would provide near-continuous monitoring of atmospheric stability at numerous locations, the sensors proposed for this network also have the potential to improve space-based retrievals. This paper will explore a

---

TABLE 1. Summary of instruments considered in this study.

Instrument	Platform	Orbit type	Horizontal resolution (km)	Spectral range	Range of instrument noise (mW m^{-2} str^{-1} cm^{-1})	Noise reference
ABI	*GOES-16*, *GOES-17*	Geostationary	2	3.90, 6.19, 6.93, 7.34, 8.44, 9.61, 10.33, 11.21, 12.29, 13.28 μm	0.0038–0.52	Schmit et al. (2017)
AERI	Multiple locations	Ground based	—	520–1800 cm^{-1}	0.01–1.8	Löhnert et al. (2009)
AIRS	*Aqua*	Polar	13.5	649–2665 cm^{-1}	0.0015–0.79	Pagano et al. (2014)
CrIS	*SNPP*, *NOAA-20*	Polar	14	650–1095, 1210–1750, 2155–2550 cm^{-1}	0.1, 0.04, 0.005	Zavyalov et al. (2013)
GIIRS/GIFTS	Fengyun-4/proposed	Geostationary	12 (GIIRS)	700–1130, 1650–2250 cm^{-1}	GIFTS noise: 0.4, 0.06	Elwell et al. (2006)
IASI	*MetOp-A*, *MetOp-B*, *MetOp-C*	Polar	12	645–2760 cm^{-1}	0.005–0.45	Hilton et al. (2012)

synergy between ground-based and space-based instruments to quantify the impacts that such a network would have on thermodynamic soundings.

Conceptually, the benefits of a combination of a space-based sounder with a ground-based sounder are intuitive. Satellite-based sounders have low information content near the surface but greater sensitivity in the middle and upper troposphere (e.g., Ebell et al. 2013; Smith and Barnet 2020). Meanwhile, ground-based instruments such as the Atmospheric Emitted Radiance Interferometer (AERI; Knuteson et al. 2004a,b) or a microwave radiometer (MWR) have information that is almost entirely contained in the lowest 4 km of the troposphere (e.g., Löhnert et al. 2009; Turner and Löhnert 2014; Blumberg et al. 2015; Turner and Löhnert 2021). The combination of the upward-pointing AERI and the downward-pointing satellite-based sensor would permit each system's strengths to be represented in the final retrieved profile.

Aires et al. (2012) showed that a synergy (both instruments in the same retrieval) provides greater improvements than a combination of individual instrument retrievals. This is because the combined retrieval allows the shared information content of the two sets of measurements to interact within the retrieval process. Ebell et al. (2013) found that the combination of the space-based Infrared Atmospheric Sounding Interferometer (IASI) and Atmospheric Microwave Sounding Unit-A/Microwave Humidity Sounder (AMSU-A/MHS) with a ground-based MWR increased the information of temperature and water vapor by a factor of 1.8 and 1.5, respectively, compared to the ground-based MWR alone. Ho et al. (2002) developed a combined retrieval between the downward-looking, aircraft-mounted Scanning High-Resolution Interferometer Sounder (S-HIS) with the ground-based AERI, finding that including AERI in the retrieval results in significant improvements in the near-surface layer compared to the S-HIS alone. Toporov and Löhnert (2020) utilized a synthetic retrieval (based on reanalysis data) combining space-based and ground-based sensors, which significantly improved CAPE calculations.

Instrument studies suggest that the space-based–ground-based synergy is a promising direction for improving thermodynamic soundings of the PBL. However, additional work remains to prove the benefits of such a synergy. Ebell et al.

(2013) simulated observations for a variety of IR and MW ground-based and space-based sensors for about 100 profiles at a single location. Their study concludes that the information content of a synergy between ground-based and space-based sensors is highly dependent upon the atmospheric state, in particular water vapor. Furthermore, while the 2017 Decadal Survey and National Research Council (2009) report set goals for the vertical resolution of soundings, instrument synergy studies have focused more on information content, leaving the vertical resolutions of both single instrument and synergistic retrievals underinvestigated. This paper will build upon the clear-sky information content study presented by Ebell et al. (2013) by conducting similar analyses in multiple climate regimes. We will also quantify the vertical resolution of single instrument retrievals from ground-based and space-based sensors and quantify the improvements offered by a synergy of the two.

2. Instrumentation

Table 1 presents a summary of the instrumentation considered in this study, which includes five different space-based IR instruments along with the ground-based AERI. We focus on IR instruments because of the greater vertical resolution and smaller footprints (allowing for a better match up with the point observations of a ground-based sensor) of IR sounders compared to MW sounders. We include three polar-orbiting space-based hyperspectral IR sounders: the Atmospheric Infrared Sounder (AIRS) on board the *Aqua* spacecraft, the Cross-track Infrared Sounder (CrIS) on board *Suomi NPP* and *NOAA-20*, and the IASI on board *MetOp-A*, *MetOp-B*, and *MetOp-C*. With the potential for hyperspectral IR sounding from geostationary orbit becoming a key component of the future observing suite, we include the proposed Geosynchronous Imaging Fourier Transform Spectrometer (GIFTS; described in Elwell et al. 2006) to explore the benefits of soundings from geostationary orbit when combined with ground-based systems. Last, we utilize the 12 IR channels on the Advanced Baseline Imager (ABI) as the only current instrument in geostationary orbit over North America offering measurements that could be used for sounding information to provide a baseline for comparison.

AIRS (launched in 2002 on board the *Aqua* satellite) and CrIS (launched in 2011 on board *Suomi NPP* and in 2017 on board *NOAA-20*) are part of the A-Train (Stephens et al. 2018) with an approximate 1330 local time equator overpass. AIRS (Chahine et al. 2006) is a grating spectrometer with 2378 channels spanning 650–2665 cm^{-1}. The instrument has a noise equivalent differential temperature ranging 0.1–0.7 K, described in Fig. 5 of Pagano et al. (2014). CrIS (Han et al. 2013) is a Michelson interferometer with three distinct spectral bands ranging from 650 to 1095 cm^{-1} with a spectral resolution of 0.625 cm^{-1}, 1210–1750 cm^{-1} with a spectral resolution of 1.25 cm^{-1}, and 2155–2550 cm^{-1} with a spectral resolution of 2.5 cm^{-1}. We utilize normal spectral resolution for CrIS instead of the full spectral resolution (which is 0.626 cm^{-1} across all three bands) because it is the resolution used in sounding retrievals (e.g., NUCAPS; Gambacorta 2013). CrIS noise is described in Fig. 1 of Zavyalov et al. (2013), ranging from approximately 0.1 mW m^{-2} sr^{-1} cm^{-1} in the long- and midwave bands to 0.01 mW m^{-2} sr^{-1} cm^{-1} in the third band.

IASI, first launched in 2006, is deployed on board *MetOp-A*, *MetOp-B*, and *MetOp-C* with equator overpass times of approximately 0930 local time. IASI, similar to CrIS, is also a Michelson interferometer. It provides continuous coverage of the radiative spectrum from 645 to 2760 cm^{-1} at a spectral resolution of 0.25 cm^{-1}. IASI's noise equivalent differential temperature is described in Fig. 3 of Hilton et al. (2012), with a range of 0.3–0.5 K at a reference temperature of 280 K. This results in noise ranging from approximately 0.1–0.45 mW m^{-2} sr^{-1} cm^{-1} in the long- and midwave bands, and 0.1 to 0.01 mW m^{-2} sr^{-1} cm^{-1} in the shortwave bands. While AIRS, CrIS and IASI are very similar instruments, we consider all three as part of our study because they differ in spectral resolution and error characteristics, which could result in different impacts on information content and the resulting synergy with ground-based instruments.

While ABI, on board *GOES-16* and *GOES-17*, only provides measurements in 12 broadband IR channels, it is the only instrument in geostationary orbit over the United States at this time that provides thermodynamic sounding information. Each of the broadband channels on ABI have sensitivity to thick layers of atmosphere (as opposed to thinner layers with hyperspectral measurements) and provide little information for sounding compared to the hyperspectral sounders. The IR channels on ABI have a spatial resolution of 2 km. ABI provides full coverage of the continental United States every 5 min, and two 1000-km mesoscale sectors every minute, which means that the benefits of a ground-based synergy would not be limited to specific overpass times.

Given the community interest in moving toward IR sounding from geostationary orbit, we consider the Geostationary Interferometric Infrared Sounder (GIIRS) that is currently in geostationary orbit on board the *Fengyun-4* satellite (Yang et al. 2017). GIIRS provides a full scan over China every 67 min, and a 1000-km mesoscale sector every 35 min. Work by Elwell et al. (2006) assessing noise characteristics of a different hyperspectral IR sounder for geostationary orbit suggest that GIIRS has greater noise than expected. Thus, we utilize noise characteristics of the GIFTS instrument, a prototype geostationary IR sounding instrument studied by NASA, the University of Wisconsin–Madison, and Utah State University (Elwell et al. 2006) in conjunction with the GIIRS spectral channels. The noise characteristics of GIFTS are closer to what is expected from the future geostationary sounders proposed by EUMETSAT and NOAA. We denote this hypothetical instrument as GIFTS throughout this paper to avoid confusion with the full characteristics of the GIIRS instrument.

AERI, the ground-based sensor in this study, is also a Michelson interferometer, similar to CrIS and IASI, that measures downwelling atmospheric emitted radiance between 520 and 3000 cm^{-1} at approximately 1 cm^{-1} resolution at better than 99% radiometric accuracy (Knuteson et al. 2004a,b). AERI measurements allow for retrievals every minute (although retrievals are typically performed at 5-min resolution) which makes it ideal for studying PBL processes (e.g., Tanamachi et al. 2008; Loveless et al. 2019; Wagner et al. 2022), as a data source for data assimilation experiments associated with severe weather (e.g., Coniglio et al. 2019; Hu et al. 2019; Degelia et al. 2020), and monitoring the temporal evolution of static stability (e.g., Wagner et al. 2008). The AERI is chosen because of its worldwide deployment in multiple climate regimes as part of the U.S. Department of Energy's Atmospheric Radiation Measurement (ARM) program (Mlawer and Turner 2016).

Previous information content analyses and retrievals utilized limited selections of the thousands of channels available on each of these instruments. We choose to consider all channels on these instruments in order to identify the full capabilities of these instruments. Utilizing the full spectral coverage of these instruments would also allow thermodynamic retrievals to overcome poor estimates of trace gases.

3. Radiosonde data

One of the areas for further exploration noted by Ebell et al. (2013) was the effect of moisture on information content of IR soundings; this was also discussed from the ground-based AERI point of view in Turner and Löhnert (2014). One of the goals of the present study is to gain an understanding of the effects of varying moisture on information content on combined ground- and space-based retrievals. Since ARM launches two to four radiosondes daily at each of its sites, we have a multiyear collected dataset consisting of radiosonde thermodynamic profiles and AERI radiance observations. As such, we utilize the ARM observation sites in the east North Atlantic (ENA; Dong et al. 2014) on the Azores islands, North Slope of Atlantic (NSA; Verlinde et al. 2016) in Barrow/Utqiaġvik, Alaska, and Southern Great Plains (SGP; Sisterson et al. 2016) in Lamont, Oklahoma. This provides our analysis with profiles from a marine subtropical environment, a polar environment, and a midlatitude continental environment in order to assess the gains in information content of a synergy of ground-based and space-based instruments in varying climate regimes. While SGP and NSA have radiosonde archives that extend back more than 15 years, ENA only

TABLE 2. Overview of radiosonde data considered for this study. Total radiosondes are the number of radiosondes in the ARM archive from 1 Oct 2013 to 30 Sep 2019.

Station	SGP	ENA	NSA
Total radiosondes	8536	4739	5037
Removed for quality control	42 (0.5%)	18 (0.4%)	15 (0.3%)
Removed for possible cloud	4617 (54.1%)	4221 (89.1%)	4506 (89.5%)
Removed for not reaching 100 hPa	112 (1.3%)	36 (0.8%)	25 (0.5%)
Total used in calculations	3765 (44.1%)	464 (9.8%)	491 (9.7%)

has radiosonde data available beginning in September 2013. To maintain uniformity, we use profiles from 1 October 2013 to 30 September 2019 for all three stations in constructing our radiosonde profile database, providing a large range of environments to simulate for our information content experiment.

Only clear-sky radiosonde profiles are used for simulation because simulating IR observations in cloudy scenes requires several orders of magnitude more calculations, making an analysis on such a large set of atmospheric profiles impractical. We flag profiles as possibly containing clouds if any relative humidity measurement in the radiosonde profile is greater than 90%. We also require a radiosonde to reach 100 hPa to ensure that the entire troposphere has been observed. Since the top of the AIRS pressure grid is 0.5 hPa and it is rare for standard radiosondes to reach that level, the radiosonde-observed profiles are augmented with the U.S. Air Force standard atmosphere geophysical model (McClatchey 1972) to provide a continuous profile up to that upper limit. This enables including the radiative contributions from the stratosphere and mesosphere in the radiative transfer calculations and preserves the lapse rates of the upper atmosphere in the model atmosphere while increasing or decreasing the temperature and water vapor mixing ratio to match the top measurement of the radiosonde. We also ensure that each radiosonde passes ARM's quality control measures [referred to as "quality control" in Table 2; the reader is directed to Peppler et al. (2016) for an overview on ARM's data quality program]. As summarized in Table 2, these quality control measures result in a dataset that consists of 464 profiles at ENA, 491 at NSA, and 3765 at SGP. SGP has many times more profiles that meet our requirements than ENA and NSA because SGP has nearly double the total number of archived radiosondes (as SGP launches four radiosondes a day while the other sites only launch two) while experiencing fewer clouds. These radiosondes are interpolated onto the 101-level AIRS pressure grid for radiative transfer modeling of the six instruments described in Table 1.

4. Radiative transfer modeling

Across the three ARM stations, this analysis considers 4720 radiosonde profiles. To make it practical to compute radiative transfer calculations over such a large number of profiles for all of the channels on each instrument, we use an optical spectral sampling (OSS) fast radiative transfer model (Moncet et al. 2008, 2015). The OSS algorithm is patented by Atmospheric Environmental Research, Inc., and calculates the channel radiance using a weighted set of monochromatic radiances based on a large training set of atmospheric and surface states (Moncet et al. 2015). The inputs to OSS are the temperature profile and constituent profiles of water vapor, carbon dioxide, trace gases in addition to skin temperature, surface emissivity, and reflectivity. The implementation of OSS used in this study produces radiances and temperature, water vapor, and trace gas Jacobians for a given atmospheric state. Currently, OSS is designed to simulate the spectral characteristics of AERI, AIRS, CrIS, and IASI. We utilize radiance and Jacobian simulations for IASI, because of its continuous coverage and high spectral resolution, to calculate those measures for ABI and GIIRS (what we are designating as GIFTS) by using their spectral response functions to the IASI channels. Radiative transfer calculations for the geostationary sensors, ABI and GIFTS, simulate those instruments from the viewing angles of *GOES-16* (longitude of 75.2°W) for SGP, and of *Meteosat-11* (longitude of 0°) for ENA. We do not simulate the geostationary sensors for NSA because of the oblique viewing angle of polar regions from geostationary orbit. The polar-orbiting sensors (AIRS, CrIS, and IASI) are simulated at nadir.

We configure OSS to account for absorption by water vapor and trace gases such as carbon dioxide, methane, ozone, and nitrous oxide. To focus on the effects that changes in the thermodynamic profiles (specifically water vapor) have on information content, similar to the study done by Ebell et al. (2013), we utilize the same trace gas concentrations for every profile, regardless of the station. A representative trace gas profile is chosen from a NUCAPS (Gambacorta 2013) retrieval over SGP, since the majority of profiles are from the SGP site. This trace gas profile is used in calculations for all 4720 profiles in the analysis. Emissivity and skin temperature are specified in the radiative transfer calculations and not included as part of the averaging kernel calculations for the satellite-based sensors in order to focus the analysis on parameters both the ground-based and space-based instruments can retrieve. The NASA Combined Aster and MODIS Emissivity for Land (CAMEL; Borbas et al. 2018; Loveless et al. 2021) monthly climatology of surface emissivity is used for each of the three stations to provide characteristic surface emissivity for the calculations.

5. Quantifying information content and vertical resolution

We will utilize the Rodgers (2000) framework for information content of a system in which an observation y can be explained as a function of the state x and error ε:

$$y = F(x) + \varepsilon, \tag{1}$$

where F is the forward model. Following Rodgers (2000) the averaging kernel $\mathbf{A}$ can be calculated by

$$\mathbf{A} = \mathbf{S}\left(\mathbf{K}^{\mathrm{T}}\mathbf{S}_e^{-1}\mathbf{K}\right), \tag{2}$$

where $\mathbf{S}_e$ is the model and measurement error covariance matrix, $\mathbf{K}$ is the Jacobian (dy/dx) and the posterior error covariance matrix $\mathbf{S}$ is

$$\mathbf{S} = \left(\mathbf{K}^{\mathrm{T}}\mathbf{S}_e^{-1}\mathbf{K} + \mathbf{S}_a^{-1}\right)^{-1}. \tag{3}$$

The a priori covariance matrix $\mathbf{S}_a$ is calculated using the radiosonde profiles such that

$$\mathbf{S}_a^{j,k} = \mathrm{CORR}(x_j, x_k)\sigma_{xj}\sigma_{xk}, \tag{4}$$

where σ_{xj} and σ_{xk} are the standard deviation of the atmospheric state (temperature or water vapor mixing ratio) at height levels j and k, respectively, and $\mathrm{CORR}(x_j, x_k)$ is the correlation between the atmospheric state at height levels j and k. Given the large differences in surface pressure across the three stations, the natural log of the ratio of the surface pressure to each pressure level is used as a vertical coordinate to ensure that the surface information from each profile is covaried together in the construction of $\mathbf{S}_a$. Matrix $\mathbf{S}_a$ is calculated as a pseudoglobal a priori where 50 profiles from each season at each station are randomly selected to form $\mathbf{S}_a$. This is displayed in Fig. 1.

As is noted in Ebell et al. (2013), this theoretical framework assumes a perfect forward model. While this is a faulty assumption, modeling errors are difficult to quantify. Ebell et al. (2013) attempts to quantify this by taking the differences in radiance calculations when each trace gas is scaled by a factor of 0.95. Comparatively, Masiello et al. (2012) uses a scaling factor to inflate $\mathbf{S}_e$. An additional problem with developing a synergy between ground-based and space-based sensors is quantifying the effect of matching a heterogeneous FOV from the space-based sensor with the point observation of the ground-based sensor. With little consensus on how to best account for sources of error, we choose to simply use the instrument noise (Table 1) error covariance $\mathbf{S}_e$. This will not only produce an overestimate of information content but (when combined with the choice to use all instrument channels) will identify the theoretical maximum in information content available from these instruments and the resulting synergy.

Smith et al. (2021) suggests performing a dry temperature retrieval on bands not sensitive to water vapor, and then performing the water vapor retrieval with the knowledge of the temperature profile. However, this method would omit temperature information contained in the water vapor channels. We choose to follow the decisions of Ebell et al. (2013) and Turner and Löhnert (2021) and calculate $\mathbf{A}$ for both temperature and water vapor simultaneously. The analysis will center on two variables that may be computed from $\mathbf{A}$: 1) the degrees of freedom (DOF), and 2) the vertical resolution of the retrieval.

1) DOF is a measure of the number of independent pieces of information contributed to the retrieval due to a signal
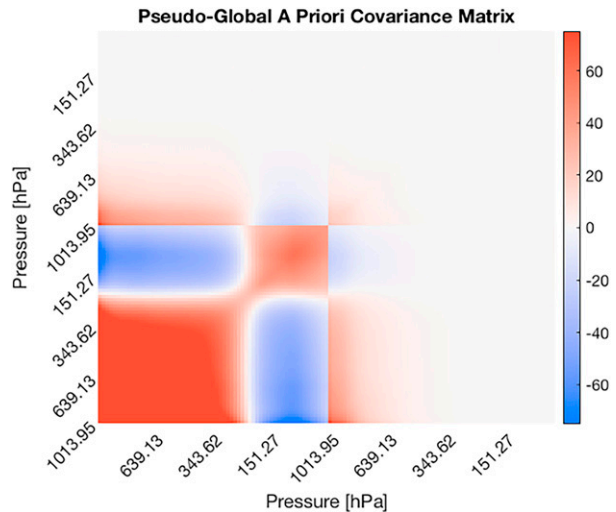

FIG. 1. A priori covariance matrix used in this analysis. (bottom left) Temperature covaried against itself (units: K^2). (top right) Water vapor varied against itself (units: $\mathrm{g\,kg}^{-2}$). (top left) Temperature and (bottom right) water vapor covaried against each other (units: $\mathrm{K\,g\,kg}^{-2}$).

from the instrument beyond what is already known from the a priori. This measure allows us to compare differences in information between different instruments and different instrument synergies, as shown in Ebell et al. (2013). DOF is calculated as the trace of $\mathbf{A}$:

$$\mathrm{DOF} = \mathrm{Trace}(\mathbf{A}). \tag{5}$$

2) The vertical resolution of a retrieval may be approximated by scaling the inverse of the diagonal elements of $\mathbf{A}$ by the vertical spacing of the grid, as shown in Hewison (2007):

$$\mathrm{Vres}_i = \frac{z_{(i-1)} - z_{(i+1)}}{\mathbf{A}_{i,i}}, \tag{6}$$

where z is the height. Note that the vertical resolution is limited by the resolution of the vertical grid that is used; in this case we chose to utilize the AIRS 101 pressure levels grid for our calculations (and the associated altitude levels provided by the radiosonde data) given its widespread use in the satellite-based sounding community, despite the coarse resolution near the surface. While this grid is appropriate to assess the vertical resolution of retrievals derived from the space-based sensors, it will result in underestimating the vertical resolution of AERI retrievals near the surface.

6. Results

a. Degrees of freedom

We begin by considering the results of the DOF analysis for all six instruments. The DOF calculations across the full troposphere (which we denote as the surface to 200 hPa) are displayed in Fig. 2. Both Ebell et al. (2013) and Blumberg
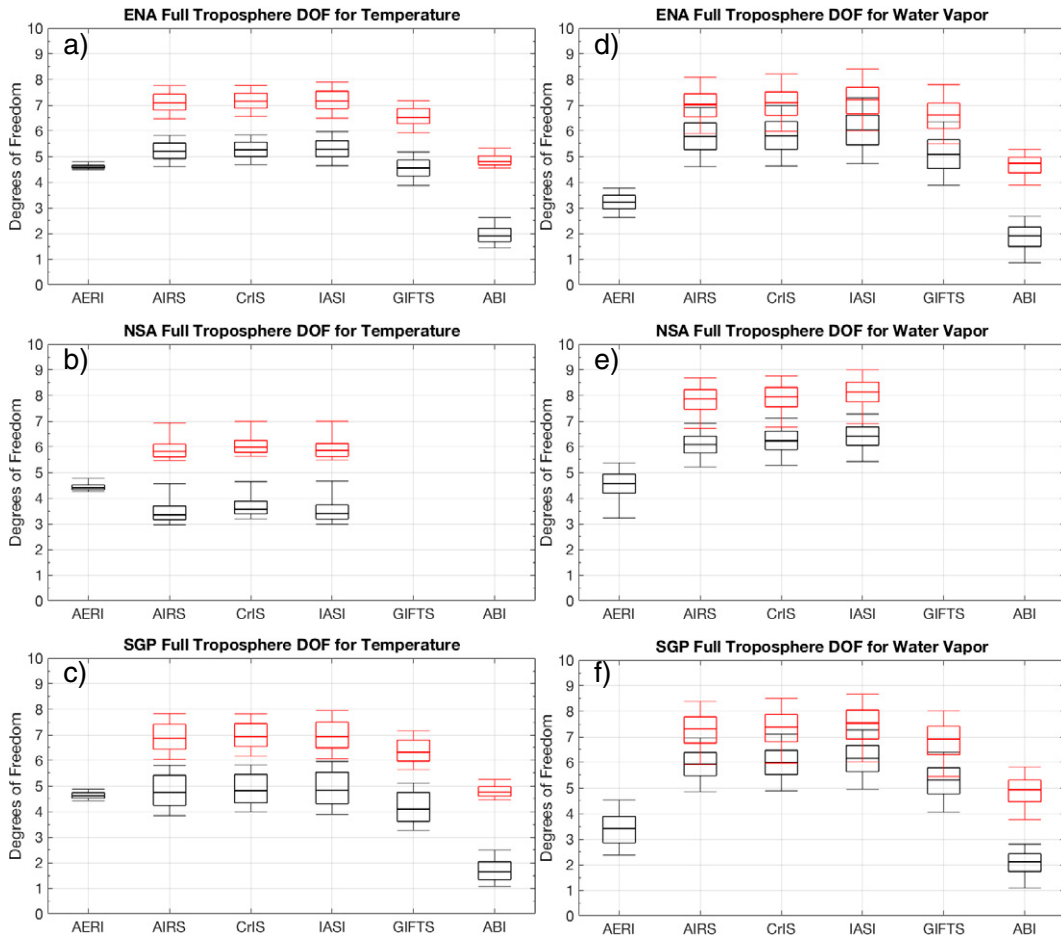
FIG. 2. DOF for (a)–(c) temperature and (d)–(f) water vapor for the full troposphere (surface to 200 hPa). DOF for the individual sensors is displayed in black. DOF for the synergy of the AERI with each respective space-based sensor is displayed in red.

et al. (2015) presented DOF calculations for AERI alone, finding roughly 5.5 DOF for temperature and roughly 3 DOF for water vapor across a similar layer, largely consistent with the full troposphere results we find for AERI. Ebell et al. (2013) finds about 4 DOF for both temperature and water vapor for IASI alone. Our methods produce about 5 DOF for temperature and 6 DOF for water vapor from IASI alone. This difference is likely attributable to the coarser grid of only 43 levels that Ebell et al. (2013) used compared to the AIRS 101 pressure levels used in this study, but channel selections, the a priori matrix, and model differences may also contribute to the differences.

Assessing the results in Fig. 2, AIRS, CrIS, and IASI (the three polar-orbiting hyperspectral sounders) all have very similar DOF to one another. While these results are nadir only, Jacobians and the resultant DOF had no significant changes with scan angle up to 35°. GIFTS has about 0.5–1 DOF less than the polar-orbiting sounders. We found that this is more of a result of the noise characteristics and the fewer total channels of the hypothetical GIFTS/GIIRS sensor

compared to the AIRS, CrIS, or IASI than the sensor angle used to simulate geostationary orbit. ABI has less than half of the information that the sounders offer, as would be expected given the relatively small number of broadband channels that it has.

The combination of AERI with the space-based hyperspectral sounders (AIRS, CrIS, GIFTS, and IASI) results in a 30%–40% increase in total DOF compared to the space-based sounder alone while the addition of AERI to the geostationary ABI results in more than doubling the information when compared to the ABI alone. The variations in DOF across the three sites are relatively small. Information content for AIRS, CrIS, and IASI at NSA is about 1 DOF lower for temperature, compared to SGP and ENA, and 1 DOF higher for water vapor. For the upward-facing AERI, profiles at NSA and SGP result in largely similar DOF for temperature, while the DOF for temperature at ENA is only marginally less. AERI gets about 4–5 DOF for water vapor at NSA, but only about 3–3.5 DOF at ENA and SGP. The synergy combinations largely follow the patterns of the space-based sensors,
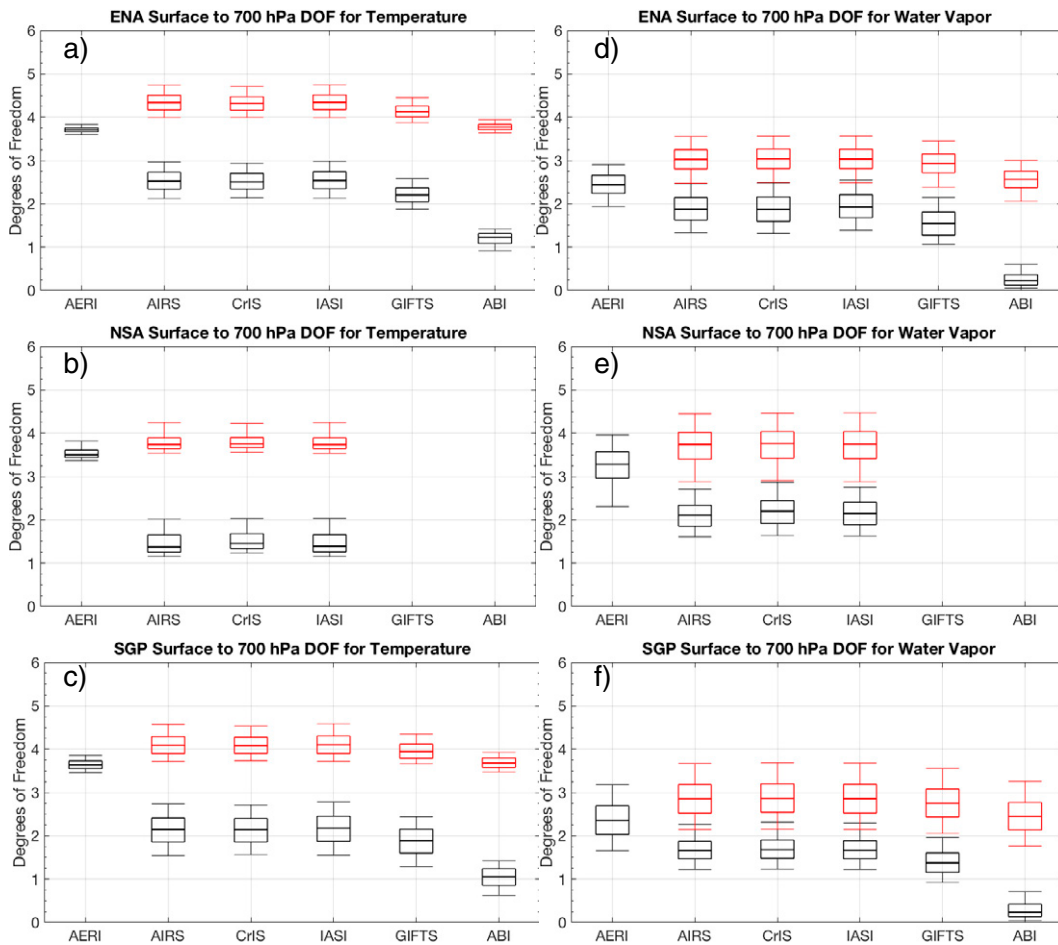
FIG. 3. As in Fig. 2, but for the surface-to-700-hPa layer.

resulting in greater temperature information at ENA and greater water vapor information at NSA.

Figure 3 focuses on the PBL and lower free troposphere by displaying DOF calculations for the surface-to-700-hPa layer. ABI only offers 1 DOF for temperature, while the space-based hyperspectral sounders produce about 1.5–2.5 DOF (more at ENA, less at NSA) for temperature in the PBL. The space-based hyperspectral sounders have about 1.5–2 DOF for water vapor while ABI has less than 0.5 DOF in the PBL. The benefits of ground-based remote sensing in the PBL are clear as AERI by itself produces about 1.5-times-greater DOF for temperature in the surface-to-700-hPa layer than any of the space-based hyperspectral sounders. However, the synergy of AERI with the space-based hyperspectral sounders promises even greater benefits, with results indicating a doubling of DOF for temperature, and an increase of about 40%–50% for DOF for water vapor as compared to the space-based hyperspectral sounders alone. AERI paired with a space-based hyperspectral sounder would result in about 4–4.5 DOF for temperature and 3–4 DOF for water vapor. This would present a significant improvement in PBL sounding, compared to what is currently provided with space-based

hyperspectral sounders alone, as the increased DOF enables the retrieval of greater detail in the structure of variations in low-level temperature and water vapor, thus producing more finely resolved inversion and moist layers. Similar to the patterns identified in the full troposphere view in Fig. 2, the space-based hyperspectral sounders provide marginally greater temperature DOF from the surface up to 700 hPa at ENA, with greatest water vapor DOF at NSA. AERI provides similar temperature information across the three sites, but greater water vapor information at NSA than at ENA or SGP. The variation of the synergies once again more closely follows the variation of the space-based sensors more than that of AERI.

b. Dependency of the information content on precipitable water vapor

While comparing DOF across the different sites may allow for broad generalizations (as ENA usually has greater atmospheric moisture content than NSA, for example), the profiles compiled for each site exhibit significant variability throughout the duration of the analyzed period so that some profiles at SGP may have greater moisture than profiles at ENA. To
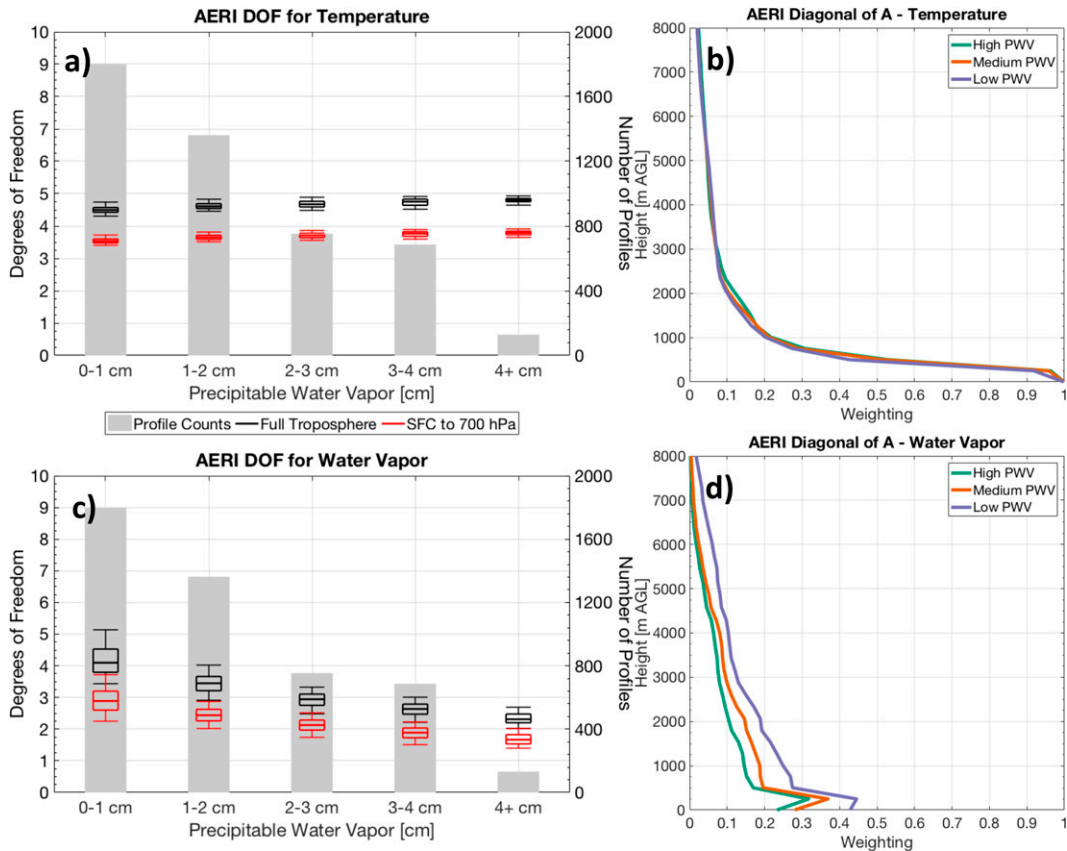
FIG. 4. AERI DOF for (a) temperature and (c) water vapor binned for every 1 cm of PWV. Number of profiles in each PWV bin is displayed as the gray bars, DOF for the full troposphere (surface to 200 hPa) is displayed in black, and the DOF for the surface to 700 hPa is displayed in red. The diagonal of high (4+ cm, green)-, medium (2–3 cm, orange)-, and low (less than 1 cm, purple)-PWV composite-mean averaging kernels for AERI for (b) temperature and (d) water vapor are shown.

gain a better understanding of the effects of moisture on information content for each of these sensors, we compute the precipitable water vapor (PWV) of each profile using SHARPpy (Blumberg et al. 2017). Given how similar AIRS, CrIS, GIFTS, and IASI are in the DOF calculations, we focus the remainder of the results section on CrIS since it is the most recent sounder put into operation by NOAA, while keeping in mind that we expect these results to be consistent with AIRS, GIFTS, and IASI. Given the relative lack of sounding information that ABI provides, we omit it from the remainder of the discussion.

To assess how DOF varies with PWV, we bin profiles for every 1 cm of PWV and compute the range of DOF for those profiles. While every PWV bin less than 4 cm contains greater than 650 profiles, the 4+ cm bin only contains 128 profiles. This 4+ cm bin still should be a large enough sample size to draw conclusions from, given that Ebell et al. (2013) had a sample of only 100 profiles.

Figure 4a displays AERI's DOF for temperature demonstrating that there is little variation in DOF with PWV at either the full troposphere view (surface to 200 hPa), or in the near-surface layer (surface to 700 hPa). Since DOF is an

integrated quantity, it is difficult to discern the heights at which the variations may be found. To determine if PWV variations cause changes in the vertical distribution of the information, we create composite mean averaging kernels from the profiles with 4+ cm of PWV (high-PWV composite), with 2–3 cm (medium composite), and with less than 1 cm (low composite). Since DOF is the trace of **A** [Eq. (5)], we can assess the changes in information at different heights by plotting the diagonal elements of the three sets of composite averaging kernels; this analysis for temperature with AERI is shown in Fig. 4b. Just as there was no variation in DOF with varying PWV, there is no difference in information at different height levels with the varying precipitable water composites. This suggests that greater water vapor amount does not result in greater attenuation of the temperature signal aloft, compared to dry environments.

However, AERI's DOF for water vapor is susceptible to changes in the PWV content of the environment, as shown in Fig. 4c. AERI has greatest water vapor DOF in dry environments, and a minimum in DOF in very moist environments; this is in agreement with Turner and Löhnert (2014). On average, there is approximately a 1.5 DOF difference between the 0–1 and the 4+ cm bin for the surface-to-200-hPa layer, and a
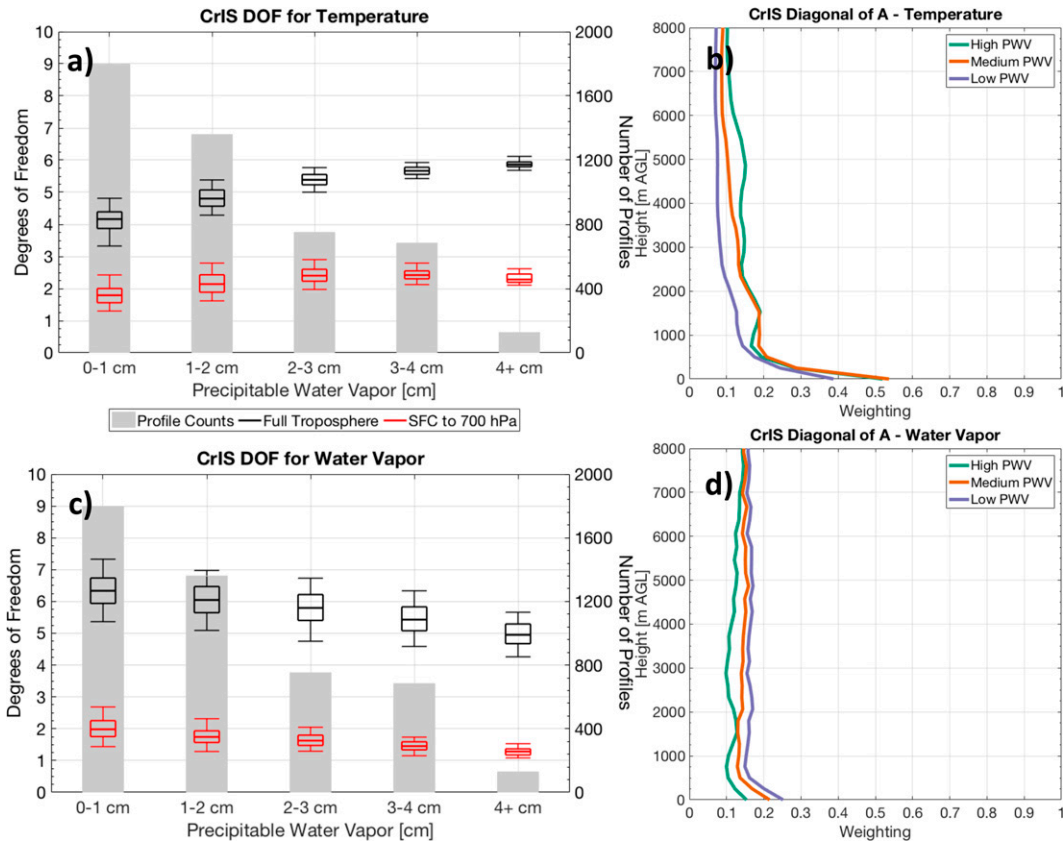
FIG. 5. As in Fig. 4, but for CrIS.

difference of about one DOF for the surface-to-700-hPa layer. Figure 4d reflects this pattern as the low PWV composite has the greatest information throughout the profile compared to the high and medium composites. This is because AERI's far IR channels (520–600 cm^{-1}) are very sensitive to water vapor in cold and dry environments. The advantages of water vapor sounding in cold and dry environments using the far IR have also been documented by Bianchini et al. (2011).

Unlike the AERI, the DOF for temperature from CrIS does vary with PWV, as is shown in Fig. 5a. Across the surface-to-200-hPa layer, CrIS has the least DOF in dry environments and maximizes DOF in the 3–4 and 4+ cm bins. The difference between the 0 and 1 and the 4+ cm bins is approximately 1.75 DOF on average. The CrIS temperature DOF for the surface-to-700-hPa layer is also at a minimum in the driest environments. However, DOF for the surface-to-700-hPa layer increases from about 1.5 in the 0–1 cm bin to 2.5 in the 2–3 cm PWV bin but remains around 2.5 for the 3–4 and 4+ cm bins as well. Figure 5b shows that the medium and high PWV composites have nearly the exact same information below 2500 m AGL (reflective of the lack of variation in CrIS temperature DOF in the surface-to-700-hPa layer between 2 and 4+ cm PWV). The difference between the medium and high composites is above 2500 m AGL, where the high composite has greater information than the medium composite, resulting in the DOF pattern in the surface-to-200-hPa layer. The low

PWV composite has the least information throughout the profile. An assessment of Jacobians for each composite reveals that this pattern is caused by greater absorption (and thus greater signal) by channels sensitive to water vapor. The greater signal from the water vapor sensitive channels supplements the existing signal for temperature from the channels that are not sensitive to water vapor, resulting in the marginal increase in DOF. However, note that if a retrieval does not include bands sensitive to water vapor for retrieving temperature (as suggested by Smith et al. 2021), then its temperature DOF will not be sensitive to variations in PWV.

Figure 5c displays CrIS DOF for water vapor with varying PWV. In general, across the surface-to-200-hPa layer, CrIS has greater DOF for water vapor in dry environments than in moist environments, opposite the pattern seen for temperature with CrIS. The median water vapor DOF in the 0–1 cm bin is about 1.5 greater than the median DOF in the 4+ cm bin. The variation in DOF across the surface-to-700-hPa layer is similar to the surface-to-200-hPa layer, with the greatest information in dry environments and the 4+ cm bin having about 0.5 DOF less than the 0–1 cm bin. Figure 5d reveals that the dry environments result in greater water vapor information throughout the profile, while the very moist environments result in the least water vapor information throughout the profile. Unlike the temperature retrieval, the water vapor retrieval cannot be supplemented with channels not sensitive
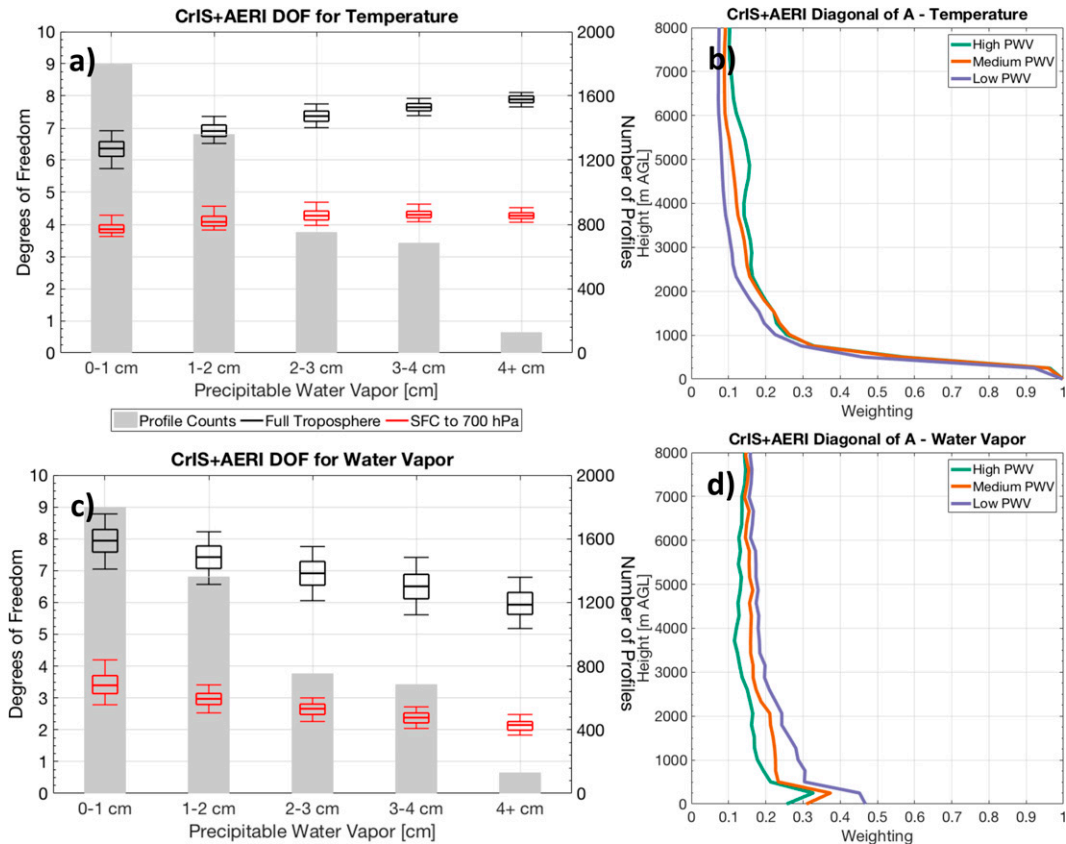
FIG. 6. As in Fig. 4, but for CrIS+AERI.

to water vapor (thus provide no signal to water vapor). Therefore, attenuation of the signal for water vapor sensitive channels results in a decrease of water vapor information with increased in PWV.

Figure 6 displays the variations in DOF and information with PWV for the synergy of CrIS and AERI (referred to as CrIS+AERI for the rest of this paper). As will be displayed in the vertical resolution and uncertainties sections, CrIS informs the synergy aloft while AERI informs the synergy very close to the surface. Figure 6a reveals that the surface-to-200-hPa DOF for temperature from CrIS+AERI varies primarily like temperature DOF for CrIS alone across the surface-to-200-hPa layer with about 1.5 DOF less in the 0–1 cm bin than in the 4+ cm bin. There is small variation across the PWV bins in the surface-to-700-hPa layer. The diagonal elements of **A** in the three composites in Fig. 6b give a sense of how AERI and CrIS are blended in the synergy. Below 500 m AGL, the information of the composites is all the same, similar to what was seen for AERI in Fig. 4b. Increasing in height from 1000 to 3000 m AGL the pattern of information transitions to reflect CrIS alone more than AERI alone, and thus the low PWV composite has less information than the high and medium composites. Above 4000 m AGL, CrIS+AERI mirror the pattern seen for CrIS alone in Fig. 5b.

As shown in Fig. 6c, the DOF for CrIS+AERI for water vapor across the surface-to-200-hPa layer has a maximum in

the 0–1 cm bin and decreases with increasing moisture to have a minimum in the 4+ cm bin. The difference in DOF between the 0–1 and the 4+ cm bins is about 2. The same pattern as was described for the DOF in the surface-to-200-hPa layer is present in the surface-to-700-hPa layer, with a difference of about 1 DOF between the maximum in the 0–1 and the 4+ cm bins. This is approximately the same difference that was seen between the same bins in Fig. 4c for AERI water vapor DOF. Figure 6d shows how AERI's sensitivity to water vapor in cold and dry environments from its far IR channels dominates the pattern in information near the surface, driving the variations seen in the DOF for the surface-to-700-hPa. This increased water vapor information from AERI's far IR channels causes the increased difference in DOF across the surface-to-200-hPa layer between the 0–1 and the 4+ cm bins compared to the pattern seen for CrIS alone.

We will conclude this section noting that despite these variations in DOF across the two layers we have considered, CrIS+AERI offers greater DOF in every PWV bin than AERI or CrIS alone. This indicates that the synergy would be expected to provide an improvement in thermodynamic sounding accuracy in all ranges of environments.

c. Vertical resolution

As noted in Eq. (6) (from Hewison 2007), the averaging kernel **A** allows for calculation the vertical resolution of a
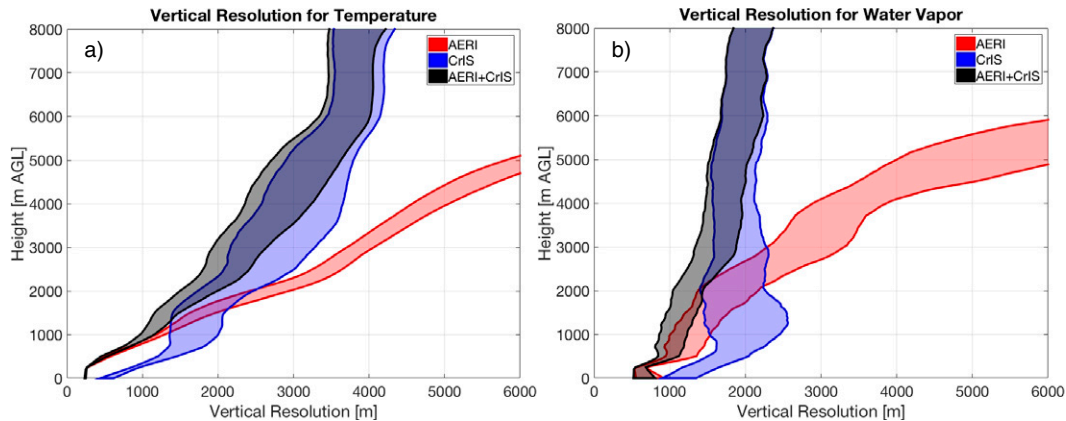
FIG. 7. Vertical resolution of (a) temperature and (b) water vapor retrievals from AERI (red) and CrIS observations (blue), and the synergy of CrIS+AERI (gray). Shading is between the 25th and 75th percentiles for all 4720 profiles in the analysis.

retrieval by spreading the diagonal elements of **A** (the same elements used to calculate DOF) across the vertical grid used for calculations. The vertical resolution of a retrieval is analogous to the thickness of the layer over which the signal is coming from when the retrieval makes an estimate at a particular level. Vertical resolution for temperature and water vapor retrievals derived from AERI, CrIS, and CrIS+AERI are shown in Fig. 7. The shadings for each sensor are between the 25th and 75th percentiles of all 4720 profiles included in this analysis. As noted earlier, the vertical resolution of a retrieval is dependent on the grid used in calculations. Since we use the AIRS 101 pressure levels, this coarser grid underestimates the vertical resolution that AERI is capable of near the surface. This can be seen when comparing our calculations for AERI's temperature resolution over the lowest 200 m of the atmosphere with those presented by Turner and Löhnert (2014) and Blumberg et al. (2015), who did their vertical resolution calculations on a grid designed for AERI. As seen in Fig. 7a, the vertical resolution of AERI below 200 m AGL is never better than about 250 m, which is the resolution of the grid near the surface. [Note that Turner and Löhnert (2014) and Blumberg et al. (2015) demonstrated that AERI's vertical resolution for temperature at any height below 1 km is approximately that height; i.e., at 50 m AGL the vertical resolution is 50 m, whereas at 500 m AGL the vertical resolution is 500 m.] Above 250 m AGL, the vertical resolution for temperature for AERI largely increases linearly with height such that it has a resolution of about 1000 m at 1000 m AGL, and 2000 m at 2000 m AGL. AERI and CrIS are comparable in vertical resolution between 1000 and 2000 m AGL, with a resolution of about 1500 m. The vertical resolution of CrIS for temperature is about 2500–3500 m through most of the free troposphere, gradually getting larger with height. CrIS+AERI provides the greatest improvements, compared to CrIS alone, in the bottom 1000 m. The synergy of CrIS+AERI results in an improvement of about 400 m in vertical resolution compared to CrIS alone in the bottom 1000 m. The synergy of the two instruments results in better vertical resolution than that of the individual instruments between about 500 and 5000 m AGL, though marginal improvements are seen all the way up to 8000 m AGL.

Vertical resolution for water vapor sounding is displayed in Fig. 7b. AERI's vertical resolution for water vapor is about 800 m at the surface and increases with height. [Again, the vertical grid chosen does matter, as the vertical resolution of the water vapor profiles from Turner and Löhnert (2014) is about 200 m at the surface and rapidly decreases to 700 m at approximately 300 m AGL, which is in rough agreement with this work.] The vertical resolution of the water vapor profiles from AERI and CrIS are comparable in the 1000–3000 m AGL range, with AERI having better resolution below, and CrIS being better aloft. Overall, vertical resolution of water vapor for CrIS is better than 2500 m throughout the lowest 8000 m of the troposphere. CrIS+AERI provides an improvement of about 400 m in resolution over the bottom 2000 m of the troposphere. Similar to what was shown in Fig. 7a for temperature, the vertical resolution of CrIS+AERI is better than either instrument individually from about 500 m up to 4000 m AGL.

The 2017 Decadal Survey set a goal of 1000 m resolution soundings, which is exceeded in the bottom 1000 m AGL for both temperature and water vapor by CrIS+AERI. Neither temperature nor water vapor sounding above 1000 m for CrIS+AERI meets the 100-m-resolution goal. However, the improvements in vertical resolution made by CrIS+AERI near the surface would improve the retrievals in the PBL, where sharp gradients in temperature and water vapor are present. These improvements will aide in detecting the strength and vertical location of the capping inversion and detecting low-level variations in water vapor—two important features that would improve monitoring of severe convection.

d. Uncertainties

The 1σ uncertainties are calculated by taking the square root of the elements of the diagonal of the posterior error covariance matrix **S**. Figure 8 displays the 1σ uncertainties for AERI, CrIS, and CrIS+AERI. The temperature uncertainties
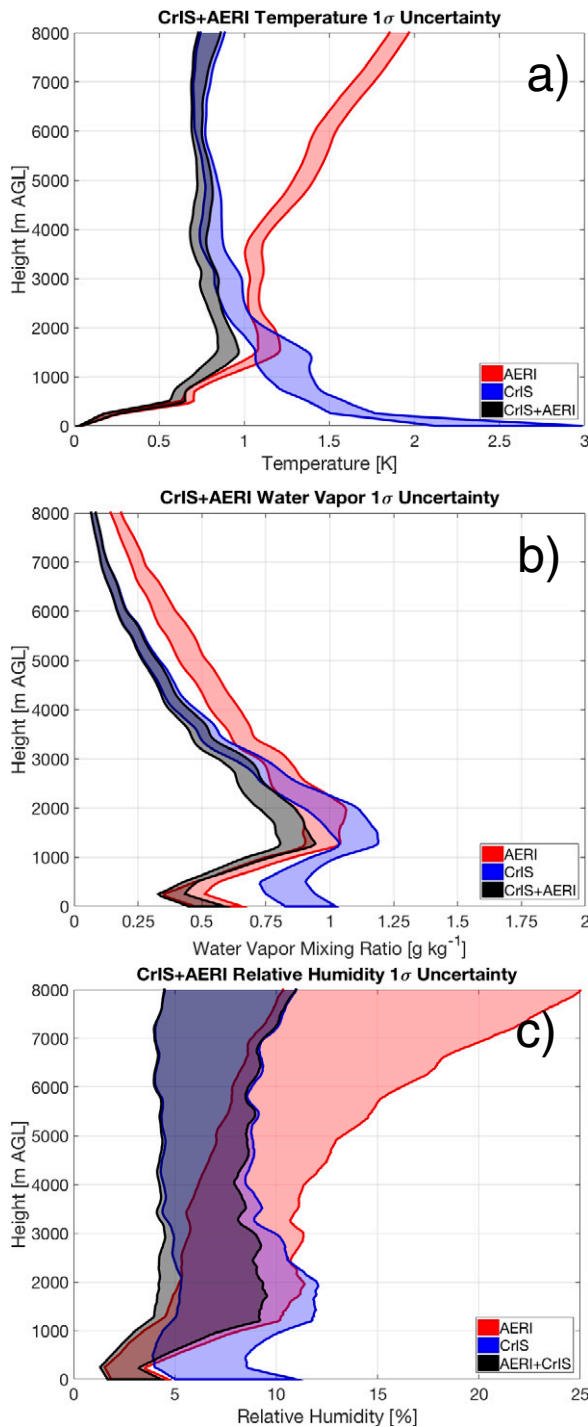
FIG. 8. The 1σ retrieval uncertainties for (a) temperature, (b) water vapor mixing ratio, and (c) relative humidity from AERI (red) and CrIS observations (blue), and the synergy of CrIS+AERI (gray). Shading is between the 25th and 75th percentiles for all 4720 profiles in the analysis. For reference, the 1σ uncertainties of the a priori are about 14 K and 4 g kg^{-1} at the surface.

of AERI increase with height while the uncertainties for CrIS are greatest near the surface, as is expected for the upward- and downward-pointing instruments, respectively. Both AERI and CrIS have a maximum in water vapor mixing ratio uncertainty at about 1000 m AGL, roughly corresponding to the mean inversion height in the radiosonde dataset used in this study. If Jacobians for an unknown skin temperature were to be included in the calculation of **A**, the near-surface uncertainties for CrIS would increase. Future work is needed to better understand the effects of skin temperature and surface emissivity on these uncertainties. Combining the temperature and water vapor mixing ratio uncertainties we consider the relative humidity uncertainties of each instrument in Fig. 8c. The relative humidity uncertainty has a maximum for CrIS at the inversion height, where its water vapor mixing ratio and temperature uncertainties are greatest as well. AERI's relative humidity uncertainty generally increases with height. The temperature and water vapor uncertainties for AERI very closely resemble the uncertainty profile displayed by Blumberg et al. (2015) and Turner and Löhnert (2014). Klein et al. (2015) also found very good agreement between the near-surface temperature in AERI retrievals and collocated in situ observations. The radiosonde validation of NUCAPS presented in Sun et al. (2017) does not identify the local maximum in uncertainty at the top of the inversion around 1000 m AGL that we identify here, which could be a product of the majority of profiles in this analysis coming from SGP. Also note that Sun et al. (2017) has differences between radiosonde and NUCAPS retrievals about 40% greater for temperature for CrIS than this study, as expected given the noise assumptions.

CrIS+AERI results in a decrease of 0.5–1.5 K or about a 50% reduction in uncertainties in the lowest 1000 m AGL, compared to CrIS alone. Similarly, CrIS+AERI results in a decrease of about 50% in the water vapor mixing ratio uncertainties and reduces the relative humidity uncertainties by half in the lowest 1000 m AGL. While the greatest improvements are in the lowest 1000 m, improvements of CrIS+AERI compared to CrIS alone occur up to 4000 m AGL. Similar to what was seen with vertical resolution, between 500 and 4000 m AGL CrIS+AERI has smaller uncertainty than either AERI or CrIS alone—again emphasizing the benefits of a combined retrieval.

Given that these instruments have far less information than the number of layers used in the radiative transfer calculations, the information gained at each level is spread over multiple levels. Similarly, uncertainties associated with one layer result in uncertainties in other layers as well. As has been shown in Turner and Blumberg (2019), the posterior correlation matrix offers a useful view to understand the improvements of an instrument synergy by looking at the cross-layer correlations in uncertainties. The posterior correlation matrices for AERI, CrIS, and CrIS+AERI are shown in Fig. 9. CrIS+AERI reduces the cross-layer sources of uncertainties compared to each instrument alone in the lowest 1000 m AGL, the same region that CrIS+AERI was shown to have the greatest improvements in vertical resolution and uncertainties.
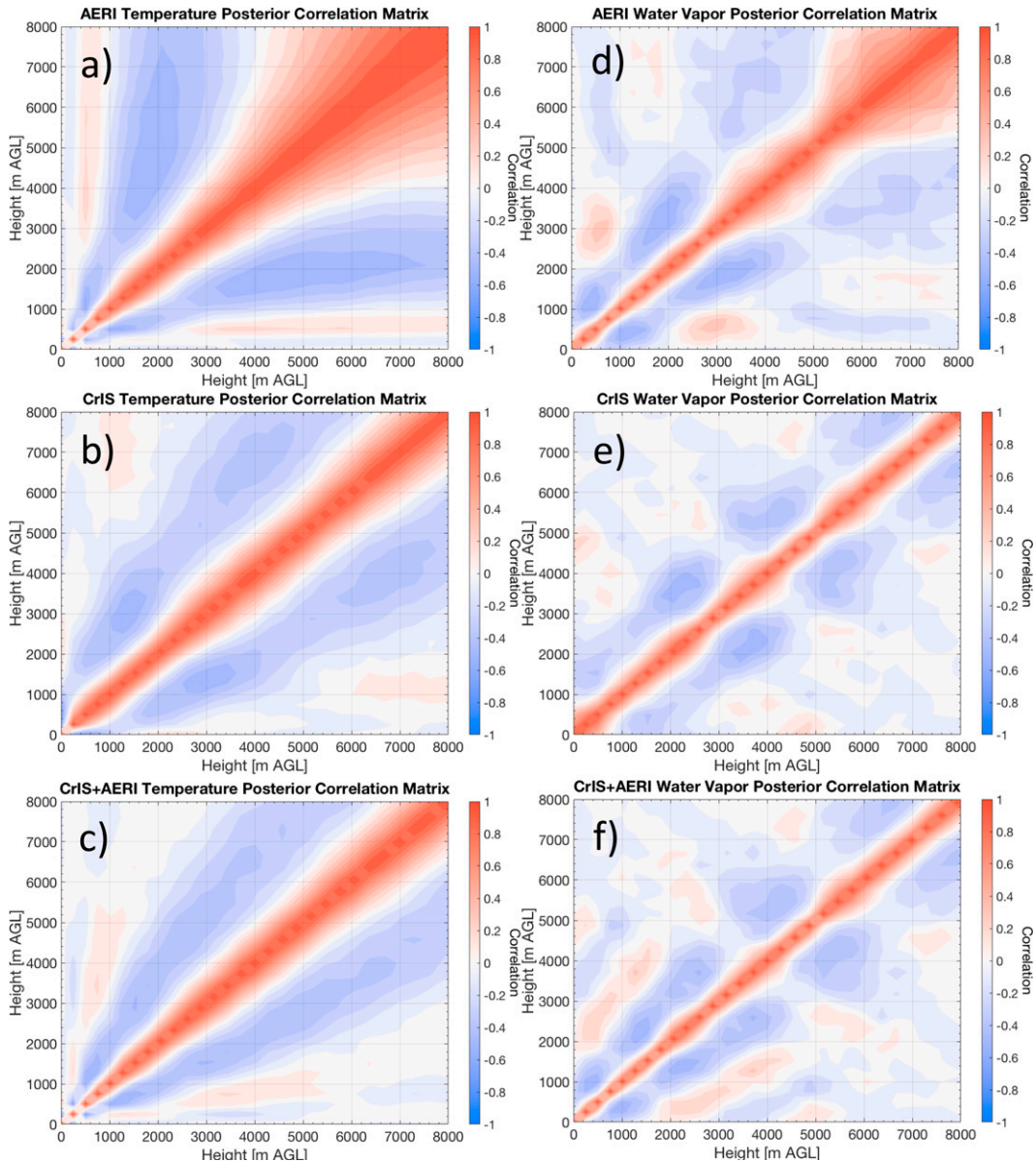
FIG. 9. Posterior correlation matrix for (a)–(c) temperature and (d)–(f) water vapor retrievals from (a),(d) AERI and (b),(e) CrIS observations, and (c),(f) the synergy of CrIS+AERI.

The improvement that the synergy offers in the lowest 1000 m compared to CrIS alone presents the case for why this ground-based–space-based synergy should be considered as a solution to the difficult problem of PBL sounding.

7. Conclusions

This study has demonstrated the benefits of combining AERI observations with the existing space-based operational hyperspectral IR sounding system. We have assessed these gains using DOF as a measure of information content and assessing the vertical resolution and uncertainties of temperature and water vapor sounding for AERI, CrIS, and CrIS+AERI for cloud-free conditions in three different climate regimes. Note, however, that the experimental design results in an overestimate of information content from only accounting for instrument noise in the error covariance matrix $\mathbf{S}_e$; uncertainties in the forward model need to be included (such as was done for the MW by Cimini et al. 2018) in future studies.

We find that including AERI in a retrieval with a space-based hyperspectral IR sounder, such as CrIS, doubles the temperature information and provides 1.5 times more information on water vapor over what is currently provided by the space-based sounders alone. We find that this improvement is consistent in both dry and moist environments, despite the ranges of information content that both sensors have across

varying PWV. The synergy of CrIS+AERI provides significant improvements to the vertical resolution over the CrIS-only retrieval below 1000 m AGL, which would improve the ability of retrievals to resolve PBL features like a capping inversion, resulting in better monitoring of convective initiation. The improvements in calculations of convective indices offered by a ground-based–space-based synergy shown by Toporov and Löhnert (2020) are likely largely due to the improvements in vertical resolution, shown in this study. CrIS+AERI also provides the greatest reductions to uncertainties in the lowest 1000 m AGL. CrIS+AERI exceeds the 1-km-vertical-resolution goal stated by the Decadal Survey in the lowest 1000 m AGL, and the 1-K-temperature uncertainty goal throughout the troposphere.

While the discussion in this paper has focused on the improvements that AERI brings to the existing sounding methods with space-based hyperspectral IR sounders, users of ground-based sensors may realize benefits of a ground-based–space-based synergy as well. We have found that the inclusion of a space-based hyperspectral IR sounder with the ground-based AERI results in about a 20% increase in DOF across the surface-to-700-hPa layer, compared to AERI alone. The synergy also offers improvements to vertical resolution and uncertainties above 500 m AGL. Given that the ABI is the only instrument currently in geostationary orbit providing nearly continuous observations over North America, it may be worthwhile for ground-based instrumentation users to consider a synergy with the ABI; similar work was done by Feltz et al. (2003) using observations from an earlier version of the GOES satellite. While we have found that a synergy with an imager like ABI does not increase the DOF near the surface (compared to AERI alone), the ABI does increase DOF by about 15% in the free troposphere.

The results of this study display the benefits of having dedicated sounding instruments in geostationary orbit. From the North American perspective, while the broadband channels on the ABI offer some sounding information, it is approximately 3–4 times less than that of a high-spectral-resolution sounder. While AERI provides near-continuous monitoring in a single location, the polar-orbiting sounders provide a spatial view of a region once every several hours. A combination of a network of AERIs with the near-constant monitoring offered by a geostationary sounder would provide the high-quality thermodynamic sounding desired by the Decadal Survey while also providing the temporal component monitoring that the National Research Council (2009) states is also crucial for improving NWP and nowcasting of high-impact weather.

While results from this study, along with those from Ebell et al. (2013) and Toporov and Löhnert (2020), have shown the promises of a ground-based–space-based synergy for thermodynamic sounding, a number of unresolved questions remain to prove the benefits of such a synergy. None of these studies address how the heterogeneous field of view of the satellite-based sensor affects the matchup with a ground-based sensor, especially since the satellite's field of view is many times larger than the ground-based sensor's. A future study could make use of the SeeBor dataset (Borbas et al. 2005) to

better understand the effects that variable skin temperature and surface emissivity over land have on the uncertainties of space-based sensors and how that may affect the space-based–ground-based synergy. Furthermore, these studies have been limited to clear-sky environments. The combination of an IR sensor above and below a cloud layer presents a solution to the problem of IR sounding in cloudy environments but those benefits need to be quantified; such an analysis is ongoing.

Data availability statement. ARM radiosondes are available in the ARM Data Discovery Archive. CAMEL emissivity product is available via the NASA Land Processes Distributed Active Archive Center (LP DAAC).

APPENDIX

List of Acronyms

ABI	Advanced Baseline Imager
AERI	Atmospheric Emitted Radiance Interferometer
AIRS	Atmospheric Infrared Sounder
AMSU-A	Atmospheric Microwave Sounding Unit-A
ARM	Atmospheric Radiation Measurement
CAMEL	NASA Combined Aster and MODIS Emissivity for Land
CAPE	Convective available potential energy
CrIS	Cross-track Infrared Sounder
DOF	Degrees of freedom
ENA	East North Atlantic
EUMETSAT	European Organisation for the Exploitation of Meteorological Satellites
IASI	Infrared Atmospheric Sounding Interferometer
GIFTS	Geosynchronous Imaging Fourier Transform Spectrometer
GIIRS	Geostationary Interferometric Infrared Sounder
MHS	Microwave Humidity Sounder
MODIS	Moderate Resolution Imaging Spectroradiometer
NAS	National Academies of Science
NASA	National Aeronautics and Space Administration
NOAA	National Oceanic and Atmospheric Administration

NRC	National Research Council
NSA	North Slope of Alaska
NUCAPS	NOAA Unique Combined Atmospheric Processing System
NWP	Numerical weather prediction
OSS	Optimal spectral sampling
PBL	Planetary boundary layer
S-HIS	Scanning High-resolution Interferometer Sounder
SGP	Southern Great Plains

REFERENCES

Aires, F., O. Aznay, C. Progent, M. Paul, and F. Bernardo, 2012: Synergistic multi-wavelength remote sensing versus a posteriori combination of retrieved products: Application for the retrieval of atmospheric profiles using MetOp-A. *J. Geophys. Res.*, **117**, D18304, https://doi.org/10.1029/2011JD017188.

Bianchini, G., L. Palchetti, G. Muscari, I. Fiorucci, P. Di Girolamo, and T. Di Iorio, 2011: Water vapor sounding with the far infrared REFIR-PAD spectroradiometer from a high-altitude ground-based station during the ECOWAR campaign. *J. Geophys. Res.*, **116**, D02310, https://doi.org/10.1029/2010JD014530.

Bloch, C., R. O. Knuteson, A. Gambacorta, N. R. Nalli, J. Gartzke, and L. Zhou, 2019: Near-real-time surface-based CAPE from merged hyperspectral IR satellite sounder and surface meteorological station data. *J. Appl. Meteor. Climatol.*, **58**, 1613–1632, https://doi.org/10.1175/JAMC-D-18-0155.1.

Blumberg, W. G., D. D. Turner, U. Löhnert, and S. Castleberry, 2015: Ground-based temperature and humidity profiling using spectral infrared and microwave observations. Part II: Actual retrieval performance in clear-sky and cloudy conditions. *J. Appl. Meteor. Climatol.*, **54**, 2305–2319, https://doi.org/10.1175/JAMC-D-15-0005.1.

——, K. T. Halbert, T. A. Supinie, P. T. Marsh, R. L. Thompson, and J. A. Hart, 2017: SHARPpy: An open-source sounding analysis toolkit for the atmospheric sciences. *Bull. Amer. Meteor. Soc.*, **98**, 1625–1636, https://doi.org/10.1175/BAMS-D-15-00309.1.

Borbas, E. E., S. W. Seemann, H. Huang, J. Li, and W. P. Menzel, 2005: Global profile training database for satellite regression retrievals with estimates of skin temperature and emissivity. *Proc. 14th Int. ATOVS Study Conf.*, Beijing, China, ITWG, 763–770.

——, G. Hulley, M. Feltz, R. Knuteson, and S. Hook, 2018: The Combined ASTER MODIS Emissivity over Land (CAMEL) part 1: Methodology and high spectral resolution application. *Remote Sens.*, **10**, 643, https://doi.org/10.3390/rs10040643.

Chahine, M. T., and Coauthors, 2006: AIRS: Improving weather forecasting and providing new data on greenhouse gases. *Bull. Amer. Meteor. Soc.*, **87**, 911–926, https://doi.org/10.1175/BAMS-87-7-911.

Cimini, D., P. W. Rosenkranz, M. Y. Tretyakov, M. A. Koshelev, and F. Romano, 2018: Uncertainty of atmospheric microwave absorption model: Impact on ground-based radiometer simulations and retrievals. *Atmos. Chem. Phys.*, **18**, 15 231–15 259, https://doi.org/10.5194/acp-18-15231-2018.

Coniglio, M. C., G. S. Romine, D. D. Turner, and R. D. Torn, 2019: Impacts of targeted AERI and Doppler lidar wind retrievals on short-term forecasts of the initiation and early evolution of thunderstorms. *Mon. Wea. Rev.*, **147**, 1149–1170, https://doi.org/10.1175/MWR-D-18-0351.1.

Degelia, S. K., X. Wang, D. J. Stensrud, and D. D. Turner, 2020: Systematic evaluation of the impact of assimilating a network of ground-based remote sensing profilers for forecasts of nocturnal convection initiation during PECAN. *Mon. Wea. Rev.*, **148**, 4703–4728, https://doi.org/10.1175/MWR-D-20-0118.1.

Dong, X., B. Xi, A. Kennedy, P. Minnis, and R. Wood, 2014: A 19-month record of marine aerosol–cloud–radiation properties derived from DOE ARM mobile facility deployment at the Azores. Part I: Cloud fraction and single-layered MBL cloud properties. *J. Climate*, **27**, 3665–3682, https://doi.org/10.1175/JCLI-D-13-00553.1.

Ebell, K., E. Orlandi, A. Hünerbein, U. Löhnert, and S. Crewell, 2013: Combining ground-based with satellite-based measurements in the atmospheric state retrieval: Assessment of the information content. *J. Geophys. Res. Atmos.*, **118**, 6940–6956, https://doi.org/10.1002/jgrd.50548.

Elwell, J. D., G. W. Cantwell, D. K. Schott, R. W. Esplin, G. B. Hansen, and S. M. Jensen, 2006: A Geosynchronous Imaging Fourier Transform Spectrometer (GIFTS) for hyperspectral atmospheric remote sensing: Instrument overview and preliminary performance results. Space Dynamics Lab Publ., 36 pp., https://digitalcommons.usu.edu/cgi/viewcontent.cgi?article=1035&context=sdl_pubs.

Feltz, W. F., W. L. Smith, H. B. Howell, R. O. Knuteson, H. Woolf, and H. E. Revercomb, 2003: Near-continuous profiling of temperature, moisture, and atmospheric stability using the Atmospheric Emitted Radiance Interferometer (AERI). *J. Appl. Meteor.*, **42**, 584–597, https://doi.org/10.1175/1520-0450(2003)042<0584:NPOTMA>2.0.CO;2.

Gambacorta, A., 2013: The NOAA unique CrIS/ATMS processing system (NUCAPS). Algorithm theoretical basis documentation. NOAA ATBD, 73 pp., http://www.ospo.noaa.gov/Products/atmosphere/soundings/nucaps/docs/NUCAPS_ATBD_20130821.pdf.

Gartzke, J., R. Knuteson, G. Przybyl, S. Ackerman, and H. Revercomb, 2017: Comparison of satellite-, model-, and radiosonde-derived convective available potential energy in the Southern Great Plains region. *J. Appl. Meteor. Climatol.*, **56**, 1499–1513, https://doi.org/10.1175/JAMC-D-16-0267.1.

Han, Y., and Coauthors, 2013: Suomi NPP CrIS measurements, sensor data record algorithm, calibration and validation activities and record data quality. *J. Geophys. Res. Atmos.*, **118**, 12 734–12 748, https://doi.org/10.1002/2013JD020344.

Hewison, T. J., 2007: 1D-VAR retrieval of temperature and humidity profiles from a ground-based microwave radiometer. *IEEE Trans. Geosci. Remote Sens.*, **45**, 2163–2168, https://doi.org/10.1109/TGRS.2007.898091.

Hilton, F., and Coauthors, 2012: Hyperspectral Earth observation from IASI: Five years of accomplishments. *Bull. Amer. Meteor. Soc.*, **93**, 347–370, https://doi.org/10.1175/BAMS-D-11-00027.1.

Ho, S., W. L. Smith, and H. Huang, 2002: Retrieval of atmospheric-temperature and water-vapor profiles by use of combined satellite and ground-based infrared spectral-radiance measurements. *J. Appl. Opt.*, **41**, 4057–4069, https://doi.org/10.1364/AO.41.004057.

Hu, J., N. Yussouf, D. D. Turner, T. A. Jones, and X. Wang, 2019: Impact of ground-based remote sensing boundary layer observation on short-term probabilistic forecasts of a tornadic supercell event. *Wea. Forecasting*, **34**, 1453–1476, https://doi.org/10.1175/WAF-D-18-0200.1.

Klein, P., and Coauthors, 2015: LABLE: A multi-institutional, student-led, atmospheric boundary layer experiment. *Bull.*

Amer. Meteor. Soc., **96**, 1743–1764, https://doi.org/10.1175/BAMS-D-13-00267.1.

Knuteson, R. O., and Coauthors, 2004a: The Atmospheric Emitted Radiance Interferometer. Part I: Instrument design. *J. Atmos. Oceanic Technol.*, **21**, 1763–1776, https://doi.org/10.1175/JTECH-1662.1.

——, and Coauthors, 2004b: The Atmospheric Emitted Radiance Interferometer. Part II: Instrument performance. *J. Atmos. Oceanic Technol.*, **21**, 1777–1789, https://doi.org/10.1175/JTECH-1663.1.

Langland, R. H., and N. L. Baker, 2004: Estimation of observation impact using the NRL atmospheric variational data assimilation adjoint system. *Tellus*, **56**, 189–201, https://doi.org/10.3402/tellusa.v56i3.14413.

LaRoche, S., and R. Sarrazin, 2010: Impact study with observations assimilated over North America and the North Pacific Ocean on the MSC global forecast system. Part I: Contribution of radiosonde, aircraft, and satellite data. *Atmos.–Ocean*, **48**, 10–25, https://doi.org/10.3137/AO1006.2010.

Löhnert, U., D. D. Turner, and S. Crewell, 2009: Ground-based temperature and humidity profiling using spectral infrared and microwave observations. Part I: Simulated retrieval performance in clear-sky conditions. *J. Appl. Meteor. Climatol.*, **48**, 1017–1032, https://doi.org/10.1175/2008JAMC2060.1.

Loveless, D. M., T. J. Wagner, D. D. Turner, S. A. Ackerman, and W. F. Feltz, 2019: A composite perspective on bore passages during the PECAN campaign. *Mon. Wea. Rev.*, **147**, 1395–1413, https://doi.org/10.1175/MWR-D-18-0291.1.

Loveless, M., E. E. Borbas, R. Knuteson, K. Cawse-Nicholson, G. Hulley, and S. Hook, 2021: Climatology of the Combined ASTER MODIS Emissivity over Land (CAMEL) version 2. *Remote Sens.*, **13**, 111, https://doi.org/10.3390/rs13010111.

Masiello, G., C. Serio, and P. Antonelli, 2012: Inversion for atmospheric thermodynamic parameters of IASA data in the principal components space. *Quart. J. Roy. Meteor. Soc.*, **138**, 103–117, https://doi.org/10.1002/qj.909.

McClatchey, R. A., 1972: Optical properties of the atmosphere. Air Force Cambridge Research Laboratories Rep., 3rd ed., 108 pp.

Mlawer, E. J., and D. D. Turner, 2016: Spectral radiation measurements and analysis in the ARM program. *The Atmospheric Radiation Measurements Program: The First 20 Years*, Meteor. Monogr., No. 57, Amer. Meteor. Soc., https://doi.org/10.1175/AMSMONOGRAPHS-D-15-0027.1.

Moncet, J., G. Uymin, A. E. Lipton, and H. E. Snell, 2008: Infrared radiance modeling by optimal spectral sampling. *J. Atmos. Sci.*, **65**, 3917–3934, https://doi.org/10.1175/2008JAS2711.1.

——, ——, P. Liang, and A. E. Lipton, 2015: Fast and accurate radiative transfer in the thermal regime by simultaneous optimal spectral sampling over all channels. *J. Atmos. Sci.*, **72**, 2622–2641, https://doi.org/10.1175/JAS-D-14-0190.1.

Nalli, N. R., and Coauthors, 2018: Validation of atmospheric profile retrievals from the SNPP NOAA-unique combined atmospheric processing system. Part I: Temperature and moisture. *IEEE Trans. Geosci. Remote Sens.*, **56**, 180–190, https://doi.org/10.1109/TGRS.2017.2744558.

National Academies of Sciences, Engineering, and Medicine, 2018: *Thriving on Our Changing Planet: A Decadal Strategy for Earth Observation from Space.* National Academies Press, 716 pp.

National Research Council, 2009: *Committee on Developing Mesoscale Meteorological Observational Capabilities to Meet Multiple National Needs.* National Academies Press, 234 pp.

Pagano, T. S., S. Broberg, H. H. Aumann, D. Elliott, E. Manning, and L. Strow, 2014: Performance status of the atmospheric infrared sounder ten years after launch. NASA JPL Rep., 9 pp., https://trs.jpl.nasa.gov/bitstream/handle/2014/42928/12-5086_A1b.pdf.

Peppler, R. A., K. E. Kehoe, J. W. Monroe, A. K. Theisen, and S. T. Moore, 2016: The ARM data quality program. *The Atmospheric Radiation Measurements Program: The First 20 Years*, Meteor. Monogr., No. 57, Amer. Meteor. Soc., https://doi.org/10.1175/AMSMONOGRAPHS-D-15-0039.1.

Rodgers, C. D., 2000: *Inverse Methods for Atmospheric Sounding: Theory and Practice.* Series on Atmospheric, Oceanic, and Planetary Physics, Vol. 2, World Scientific, 238 pp.

Schmit, T. J., P. Griffith, M. M. Gunshor, J. M. Daniels, S. J. Goodman, and W. J. Lebair, 2017: A closer look at the ABI on the GOES-R series. *Bull. Amer. Meteor. Soc.*, **98**, 681–698, https://doi.org/10.1175/BAMS-D-15-00230.1.

Sisterson, D. L., R. A. Peppler, T. S. Cressm, P. J. Lamb, and D. D. Turner, 2016: The ARM Southern Great Plains (SGP) site. *The Atmospheric Radiation Measurements Program: The First 20 Years*, Meteor. Monogr., No. 57, Amer. Meteor. Soc., https://doi.org/10.1175/AMSMONOGRAPHS-D-16-0004.1.

Smith, N., and C. D. Barnet, 2020: CLIMCAPS observing capability for temperature, moisture and trace gases from AIRS/AMSU and CrIS/ATMS. *Atmos. Meas. Tech.*, **13**, 4437–4459, https://doi.org/10.5194/amt-13-4437-2020.

Smith, W. L., H. Revercomb, E. Weisz, D. Tobin, R. Knuteson, J. Taylor, and W. P. Menzel, 2021: Hyperspectral satellite radiance atmospheric profile information content and its dependence on spectrometer technology. *IEEE J. Sel. Top. Appl. Earth Obs. Remote Sens.*, **14**, 4720–4736, https://doi.org/10.1109/JSTARS.2021.3073482.

Stephens, G., D. Winker, J. Pelon, C. Trepte, D. Vane, C. Yuhas, T. L'Ecuyer, and M. Lebsock, 2018: *CloudSat* and *CALIPSO* within the A-Train: Ten years of actively observing the Earth system. *Bull. Amer. Meteor. Soc.*, **99**, 569–581, https://doi.org/10.1175/BAMS-D-16-0324.1.

Sun, B., A. Reale, F. H. Tilley, M. E. Pettey, N. R. Nalli, and C. D. Barnet, 2017: Assessment of NUCAPS S-NPP CrIS/ATMS sounding products using reference and conventional radiosonde observations. *IEEE J. Sel. Top. Appl. Earth Obs. Remote Sens.*, **10**, 2499–2509, https://doi.org/10.1109/JSTARS.2017.2670504.

Tanamachi, R. L., W. F. Feltz, and M. Xue, 2008: Observations and numerical simulation of upper boundary layer rapid drying and moistening events during the International H_2O Project (IHOP_2002). *Mon. Wea. Rev.*, **136**, 3106–3120, https://doi.org/10.1175/2008MWR2204.1.

Toporov, M., and U. Löhnert, 2020: Synergy of satellite- and ground-based observations for continuous monitoring of atmospheric stability, liquid water path, and integrated water vapor: Theoretical evaluations using reanalysis and neural networks. *J. Appl. Meteor. Climatol.*, **59**, 1153–1170, https://doi.org/10.1175/JAMC-D-19-0169.1.

Turner, D. D., and U. Löhnert, 2014: Information content and uncertainties in thermodynamic profiles and liquid cloud properties retrieved from the ground-based Atmospheric Emitted Radiance Interferometer (AERI). *J. Appl. Meteor. Climatol.*, **53**, 752–771, https://doi.org/10.1175/JAMC-D-13-0126.1.

——, and W. G. Blumberg, 2019: Improvements to the AERIoe thermodynamic profile retrieval algorithm. *IEEE J. Sel. Top. Appl. Earth Obs. Remote Sens.*, **12**, 1339–1354, https://doi.org/10.1109/JSTARS.2018.2874968.

——, and U. Löhnert, 2021: Ground-based temperature and humidity profiling: Combining active and passive remote sensors. *Atmos. Meas. Tech.*, **14**, 3033–3048, https://doi.org/10.5194/amt-14-3033-2021.

Verlinde, J., B. D. Zak, M. D. Shupe, M. D. Ivey, and K. Stamnes, 2016: The ARM North Slope of Alaska sites. *The Atmospheric Radiation Measurements Program: The First 20 Years*, Meteor. Monogr., No. 57, Amer. Meteor. Soc., https://doi.org/10.1175/AMSMONOGRAPHS-D-15-0023.1.

Wagner, T. J., W. F. Feltz, and S. A. Ackerman, 2008: The temporal evolution of convective indices in storm-producing environments. *Wea. Forecasting*, **23**, 786–794, https://doi.org/10.1175/2008WAF2007046.1.

——, A. C. Czarnetzki, M. Christiansen, R. B. Pierce, C. O. Stainer, A. F. Dickens, and E. W. Eloranta, 2022: Observations of the development and vertical structure of the lake breeze circulation during the 2017 Lake Michigan ozone study. *J. Atmos. Sci.*, **79**, 1005–1020, https://doi.org/10.1175/JAS-D-20-0297.1.

Yang, J., Z. Zhang, C. Wei, F. Lu, and Q. Guo, 2017: Introducing the new generation of Chinese geostationary weather satellites, Fengyun-4. *Bull. Amer. Meteor. Soc.*, **98**, 1637–1658, https://doi.org/10.1175/BAMS-D-16-0065.1.

Zavyalov, V., and Coauthors, 2013: Noise performance of the CrIS instrument. *J. Geophys. Res. Atmos.*, **118**, 13 108–13 120, https://doi.org/10.1002/2013JD020457.